Langmuir **26**, 16271-16277 (2010). http://pubs.acs.org/doi/full/10.1021/la101317s

Prospects for resolving chemical structure by atomic force microscopy: a first principles study

Chun-Sheng Guo[1], *Michel A. Van Hove**[,1], *Rui-Qin Zhang*[1] *and Christian Minot*[1,2]

[1]Department of Physics and Materials Science, City University of Hong Kong, Hong Kong SAR, China

[2]Laboratoire de Chimie Théorique, Université Pierre & Marie Curie, Paris 6, CNRS, UMR7616, Case 137, 4 place Jussieu, Paris, F-75252 Cedex France

*Corresponding author. Email: vanhove@cityu.edu.hk

RECEIVED DATE (to be automatically inserted after your manuscript is accepted if required according to the journal that you are submitting your paper to)

Abstract

In a recent paper, the chemical structure of a molecule was resolved by means of atomic force microscopy (AFM): using a metal tip terminated in a CO molecule, the authors could image the internal bonding arrangement of a pentacene molecule with remarkable spatial resolution (notably better than with other tip terminations), as verified by their first-principles calculations. Here we further explore with first-principles calculations the mechanisms, applicability and capabilities of this approach for a wider range of situations, by varying the imaged molecule and the tip beyond the experimental cases. In our simulations, a high atomic resolution is found to be dominated by the electronic structure of the last two atoms on the tip apex which are set perpendicularly to the sample molecule. For example, tips terminated in CH_4 or pentacene itself (both having a C-H apex) yield similar images, while tips terminated in O_2 or CO give quite different images. While using a CO-terminated tip successfully resolves the chemical structure of pentacene and of other extended planar networks based on C_6 rings, this tip fails to resolve the structures of benzene (with its single C_6 ring) or non-planar C_6 networks, such as C_{60} or small-diameter carbon nanotubes. Defects (such as N substitution for a C-H group) were also found to significantly influence the image resolution. Our findings indicate that further application of this approach requires, for each sample, careful selection of a suitable "imaging" molecule as tip termination.

Introduction

Scanning probe microscopy is a very powerful technique that uses sharp tips to image, measure and manipulate matter at surfaces.[1, 2] Atomic resolution images can be taken with both the scanning tunneling microscope (STM) and the atomic force microscope (AFM).[3] The STM detects a current of electrons that tunnel quantum-mechanically through the vacuum gap between a voltage-biased metallic tip and a conductive surface. This tunneling current strongly depends both on atomic-scale variations of the surface topography and on electronic structure near the Fermi level. However, single atom resolution within a molecule by STM is still a great challenge, because the spatial distribution of the electronic structure can mask the "atomic structure" as defined by the individual nuclear positions. In high-resolution AFM, imaging is based on detecting the forces near the onset of the short-range bonding interaction between the sample atoms and the foremost atom of a sharp tip at the end of a cantilever. Atomic resolution has been achieved for single-walled carbon nanotubes with AFM.[4, 5] Atomic resolution with chemical identification[6] and measurement of the magnetic exchange force with AFM[7] were also achieved. Strikingly, the complete chemical structure imaging of a molecule was accomplished recently with AFM, namely for an individual pentacene molecule ($C_{22}H_{14}$, containing five fused C_6 rings).[8] At a low temperature (5 K) and using noncontact AFM in frequency modulation (FM) mode[9] with a high stiffness cantilever, the C_6 rings and even the C-H bonds within the pentacene were successfully resolved with a tip terminated with a single CO molecule.[8]

The ability to image individual molecules with such resolution is so far unique to this AFM based technique. To our knowledge, relatively few tip conditions and sample molecules have been explored experimentally, including tips terminated with CO, Cl and pentacene, limited to imaging a sample of pentacene molecules adsorbed on a few substrates.[8] It is of interest to ask what are the mechanisms, applicability and capabilities of this approach for high-resolution AFM imaging in a wider range of situations, including various sample molecules and various tips. To explore this question, we have

therefore conducted first-principles calculations for a range of tip structures and sample molecules.

Methodology

Measurement in AFM is based on detecting the forces between the foremost atoms of the sharp tip and the atoms at the surface. Operating the AFM in FM mode, a cantilever with stiffness k_0 is driven at its fundamental resonance frequency f_0 while keeping the oscillation amplitude constant during scanning. As the tip gets close to the sample, the average tip-sample force gradient alters the resonance frequency. The frequency shift is measured and mapped and thus represents the local force gradient rather than the force itself.

The forces between closed-shell atoms and molecules are primarily determined by the outer regions of the atoms, in which the atomic electron densities overlap. During AFM scanning the overlap induces a surface corrugation and results in an image that depends on both sample and tip. The force and force gradient between tip and sample can be calculated by numerical differentiation from the interaction energy (*IE*) of the tip-sample system.[6, 8] The *IE* is defined as $IE = E_{t+s} - (E_t + E_s)$, where E_t, E_s and E_{t+s} are the total energies of the tip alone, the sample molecule alone, and the combined tip-sample system, respectively. The first derivative of *IE* with respect to the tip-sample distance *d* gives the interaction force (*IF*) in the z-direction of tip motion, which force results from a combination of repulsive short range chemical forces and attractive long range forces: $IF_z = -\frac{\partial IE}{\partial d}$. The second derivative of *IE* with respect to *d* yields the frequency shift (*FS*) of the AFM cantilever: $FS = -\frac{f_0}{2k_0}\frac{\partial IF_z}{\partial d}$, where f_0 is the resonant frequency when IF_z=0 and k_0 is the stiffness of the cantilever.

Our total energy calculations (of similar level as those of Ref. 8) were performed using the efficient code package SIESTA,[10, 11] which is based on density functional theory (DFT) and a localized linear combination of atomic orbitals (LCAO) basis set that describes valence electrons and adopts norm-

conserving nonlocal pseudopotentials for the atomic cores.[12] The nonlocal components of the pseudopotential were expressed in the fully separable form of Kleiman and Bylander.[13] The total energy was calculated within the Perdew-Burke-Ernzerhof (PBE) form of the generalized gradient approximation (GGA).[14] The atomic orbital basis set employed throughout this work was a double-ζ basis with polarization (DZP) and a cutoff of 250 Ry. Van der Waals forces were added semiempirically to the dispersion energy as a contribution proportional to d^{-6} (where d is the interatomic distance),[15] which has been shown suitable for our tip-sample pair systems.[8, 16] The tip atoms and the sample molecule were fully relaxed separately until a force tolerance of 0.02 eV/Å was achieved, and then brought together for energy calculations with fixed atomic positions, because further relaxing the atoms did not noticeably change the results.[8] To obtain a 2-dimensional (2D) energy map, we fixed the tip-sample distance (as was done in the experiment) and calculated data points in a 2D box above the sample molecule.

Results and discussion

The tip-sample system in the AFM measurement with a CO-terminated tip[8] can be modeled by a metal-CO-sample-substrate group. To model the sample on the substrate, we employed a pentacene lying "horizontally" on a NaCl(100) surface of 2 monolayers (ML) thickness. In view of the rigidity of the NaCl lattice, we fixed the substrate and relaxed the rest of the system. The relaxed distance between the pentacene plane and the NaCl surface is approximately 3.6 Å, and the pentacene molecule is slightly bent along the long axis (its two ends are farther from the substrate than the central part), with a maximum height difference of around 0.1 Å between the carbon atoms in the pentacene plane. To model the tip we chose a cluster with "vertical" Au_3Au-CO structure, as shown in Figure 1a (Au is believed to coat the experimental Cu tip). The height of the tip above the molecule is 2.7 Å, which is defined as the vertical distance between the lowest atom on the tip (here the O atom) and the top atom of the sample molecule. The vertical distance from the lowest tip Au atom above CO to the pentacene plane is 5.8 Å.

We first analyze the contributions to *IE* from different parts of the system. To that end, we calculated line profiles of *IE* (Figure 1b) above the long axis of the pentacene molecule on the NaCl surface with the complete metal(M)-CO tip, and then removed the CO or the metallic parts (without changing the heights of the remaining parts over the sample). We also calculated the line profiles of *IE* on an isolated pentacene molecule with M-CO and CO tips. Firstly, we found the effect of the NaCl substrate to be negligible: the line profile of the "M-CO-pen-sub" system is almost identical to that of the "M-CO-pen" system, and the fluctuation is negligible in the line profile of the "M-CO-sub" system. Secondly, the contribution of the metallic part in the tip is small. At the central hollow site of the molecule without substrate (see "Center" site in Figure 2d), the interaction energy for the complete tip was $IE_{\text{M-CO-pen}}$ = -242 meV, while that resulting from removal of the CO molecule was $IE_{\text{M-pen}}$ = -61 meV. The difference between these *IE* values was a little smaller than for the CO-only tip, $IE_{\text{CO-pen}}$ = -218 meV, due to the interaction between the CO part and the Au_3Au part within the tip. This indicates that the metallic part Au_3Au contributes about 25% to the *IE*, comparable with the 30%[8] found experimentally. The line profiles of the M-CO and CO tips exhibit 5 *IE* minima over the centers of the 5 C_6 rings within the pentacene molecule, and 2 further *IE* minima corresponding to a halo around the pentacene molecule.[8] However, the metallic part yielded only a very small corrugation on the atomic scale (Figure 1b). Using a CO tip with vs. without a metallic part, no significant difference was found in our simulations. Based on these results, in the following we ignore the substrate and assume an undistorted planar pentacene molecule oriented "horizontally", because the bent pentacene does not result in a significant difference in the AFM image compared to a planar one in our simulations. Additionally, we simply model the tip with an isolated reactive molecule in most cases, while the effect of the metallic part is discussed only when it gets so close to the sample molecule that it affects the atomic resolution. Metallic tips (Cu, Al, etc) without reactive molecule on their apex are not discussed in this paper, because such tips prefer to chemically bond to the sample molecule in our simulations, indicating that they could move the sample molecule rather than image its atomic structure, as found in

the experiment.[8]

As the authors of the recent AFM study of pentacene [Ref. 8] have noted and utilized, there is a systematic similarity of appearance between *IE* and *FS* maps. This can be exploited to avoid calculating the relatively very compute-intensive *FS* maps by instead using carefully selected *IE* maps in evaluating the general capabilities of AFM.

This similarity can be understood and justified as follows. *IE* vs. height curves of the CO tip at different sites over the pentacene are shown in Figure 2a. The minima of *IE* at different sites fall in the range from 2.75 Å to 3.05 Å, with values on the order of -200 meV. By differentiation, we obtain the corresponding *IF* vs. height curves at those sites shown in Figure 2b. Because of their approximate Lennard-Jones shape, differentiation of the *IE* vs. height curves (Figure 2a) produces *IF* vs. height curves that have a very similar Lennard-Jones-like shape, but offset toward greater height (Figure 2b). In turn, the second derivatives give *FS* vs height curves with again a very similar shape, offset toward even greater height (Figure 2c). The absolute values of the strongest attractive forces ($IF < 0$) are on the order of 100 pN at those sites. The strongest force is found at the central hollow site, around 120 pN, while above the C13 and C13a carbon atom sites (Figure 2d) the forces are a little smaller, around 90 pN; these values agree well with experimental force results at the minimum experimental tip height (below which the imaging became unstable).[8] The respective *FS* curves, proportional to the second derivatives of *IE*, are shown in Figure 2c. (Because the frequency shift *FS* depends on the particular resonant frequency f_0 and stiffness k_0 of the cantilever in a specific AFM instrument, we chose to normalize the maximum *FS* value to be -7 Hz to match the maximum experimental[8] value for *FS* of around -7 Hz for imaging a pentacene on Cu substrate with CO tip.) We now can see that the *FS*-vs-height behavior is very similar to the *IE*-vs-height behavior for every site probed in Figure 2, with an offset in tip height: in particular, the minima of the *FS* curves occur about 0.9 Å higher above the surface than for *IE* curves in our calculations.

To compare theory with experiment, it is necessary to specify a tip-sample separation in the calculations, which however is not directly available from the experiment. Our approach is to best match the site-to-site contrast across the molecule between experiment and theory as a function of the tip-sample separation used in our calculations. For instance, the experimental result in Figure 2e has about the same *FS* values (shown as gray scale which we digitized[17] from the experimental image) at the central hollow site and at the α site between a pair of H (Figure 2d): this is matched best by our theoretical results in Figure 2c for a height of 3.55 Å, suggesting that this height value in our calculations best reproduces experiment. However, the *FS* difference among sites (Figure 2d) is very small. This may be due to the absence of effects due to the substrate, as evidenced experimentally by the fact that a NaCl substrate, which gives a weaker tip-sample interaction, results in much less pronounced *FS* contrast than a Cu substrate.[8]

Benefiting from the distinctive similarity of *IE* and *FS* curves, it can be conjectured that the *IE* map for H = 2.68 Å looks similar to the *FS* map for H = 3.55 Å, which in turn looks similar to the experimental *FS* map. This is also supported by the strong similarity of the *IE* map at 2.7 Å (Figure 2f) and the experimental AFM image (Figure 2e). The energy map was sampled with 55 × 31 data points in a box of 22.0 Å × 12.4 Å above the pentacene molecule with CO tip, then smoothly interpolated to 440 × 248 points. In the *IE* image, the central hollow site is the darkest position, with *IE* value close to the α sites (around -200 meV). Internal carbon atoms and C-C bonds have similar brightness (around -120 meV) while the carbons and C-C bonds at the two ends are brighter. Additionally, faint carbon-hydrogen bonds between two α sites are imaged and the whole molecule is surrounded by a dark halo, as in the experimental image.

Figure 3 shows interaction energy *IE* maps of pentacene with a CO tip at different heights. At a height of 2.4 Å, the minima above the C_6 ring centers are pronounced and the C-H bonds are also relatively well imaged. This suggests that the chemical structure can be well resolved at a CO height

smaller than 3.55 Å (due to shifting to increased height for a corresponding *FS* contrast), while the *FS* minima are located at α sites. However, the repulsive force over the C_6 ring below a height of 3.1 Å (Figure 2b) increases rapidly which may prevent the tip getting closer. The best contrast (especially for the C-H bonds) is found around a CO height of 2.7 Å. At the "best-resolution height" of 2.95 Å, which is the average value of the heights at which *IE* minima occur at different positions, the energy map always gives a useful contrast across the molecule. The atomic resolution is lost at 3.4 Å even for the deep hollow sites. The rapid change of the *IE* dependence on height thus results in a relatively small height window in which the chemical structure of the pentacene molecule can be imaged by means of *IE*. Similarly, the height window for atomic resolution with *FS* imaging should also be small (after a shift to increased height). The narrow height window for spatial resolution is also reported in the experiment (Figure 3A in reference 8).

In the experiments of Ref. 8, only tips terminated in CO, Cl and pentacene were considered. Here we vary the tip systematically above a pentacene molecule to discuss the influence on resolution of tip modification. Firstly we replace the CO by CH_4 and CCl_4 molecules, thus essentially replacing the end O of CO by H and Cl, resp. Secondly we replace the CO by an O_2 molecule and by a Cu_3CuO cluster, so the end atom is still O, and finally the CO is replaced by N_2 and Cl_2. In all these cases, the two atoms nearest the sample are oriented "vertically", i.e. perpendicularly to the sample molecule and the surface.

The line profiles along the long axis of the pentacene molecule obtained with the CH_4 tip (Figure 4a) are similar to those obtained with the CO tip (Figure 1b). The line profiles at different heights reveal basic information of the tip-sample interaction. For example, the minima of *IE* at any height are located at the hollow sites, and the minimum *IE* at the central hollow site is around -270 meV at 2.3 Å. Similar to CO, the CH_4 line profiles for *IF* and *FS* have similar corrugations but with shifts to increased heights (not shown). While the *IE* profile along the long axis with the CH_4 tip is analogous to that of the CO tip, the full *IE* map (Figure 4a) obtained with CH_4 tip is quite different at the "best-resolution height" of 2.5

Å. For example, the *IE* above the C13 site is close to that above the H site but much smaller than that above the C13a site. Consequently, the image of the hexagonal C_6 ring looks like parallel lines over the C-C bonds, which is similar to the experimental image with a pentacene-terminated tip (Figure 2D in Ref. 8). In fact, we obtained a similar image by employing a tilted pentacene tip oriented such that a C-H group (i.e. C2-H in Figure 2d) at one end is "vertical" and points to the sample pentacene molecule. Based on this result, we conjecture that the experimental pentacene tip has a single C-H bond pointing (more or less) toward the pentacene molecule which yields an image typical of any C-H apex. The CCl_4 tip yields a very different image from CH_4. As shown in Figure 4b, the *IE* minima are no longer located above the hollow sites but over the C_6 rings. The minimum *IE* at the central hollow site is around -140 meV at 3.2 Å while the minimum near the C13 site is around -170 meV. Although the CCl_4 *IE* map resolves the five C_6 rings, the image contrast is reversed compared with that obtained with the CO tip. At the "best-resolution height" of 3.3 Å, the *IE* corrugation of the CCl_4 tip is smaller than that of the CO tip at 2.95 Å, 20 meV vs. 50 meV (*IE* difference between the C-C bond and the hollow site), which means that the CCl_4 tip yields a less pronounced intramolecular contrast.

By replacing the CO tip with an O_2 molecule (Figure 4c), we can investigate the influence of the second-last atom on the apex. Ignoring the fact that an O_2 molecule will probably not freely stand on a metallic surface, we nonetheless orient it perpendicularly to the pentacene just like the CO. The *IE* corrugation is strong (50 meV at 2.9 Å) along the long axis, but it causes very high contrast over the C-H atoms around the hexagonal C_6 rings, making it difficult to recognize them. Considering that the O_2 molecule may dissociate on the metal surface, we further considered a tip with a Cu_3CuO cluster to model a single O atom adsorbed at a Cu apex atom of a Cu_4 tetrahedron representing fcc Cu (Figure 4d). The corrugation of *IE* at the center section reflects the central three hollow sites, but it is very weak at the two ends. The *IE* map in Figure 4d vaguely shows the three C_6 rings in the center while the two ends of the pentacene are confused.

An N_2 tip image (Figure 4e) resembles that from the CO tip, and N_2 is more likely than O_2 to adsorb perpendicularly to a metal surface. The line profile along the long axis clearly reveals the five hollows, and the minimum of *IE* at the central carbon ring is around -100 meV at a tip height of 3.3 Å (Figure 4e). While the absolute *IE* values are smaller for N_2, the difference among *IE* values at different sites is the same for the N_2 and CO tips. Consequently, the 2D energy map taken at a height of 3.3 Å gives an analogous contrast to that of the CO tip at 2.95 Å.

Line profiles produced by a Cl_2 tip (Figure 4f) are analogous to those from a CCl_4 tip; there are local *IE* maxima over hollow sites and minima over the C_6 rings, while the halo around the molecule is more significant than that yielded by other tips discussed above at smaller heights, because the *IE* minima responsible for the halo around the molecule have lower values than over the C-C bonds. The 2D energy map taken at the "best-resolution height" of 3.3 Å resolves the five C_6 rings. As for the CCl_4 tip, the contrast is reversed compared to that for the CO tip.

In vacuum, the force between tip and sample atoms is ascribed to short-range chemical forces, Van der Waals forces and static electronic forces in a non-magnetic system. The atomic resolution in AFM is based on detecting the short-range chemical forces, while the Van der Waals and static electronic forces are small in this case.[8, 18] If we assume that the AFM *FS* image is taken around a height of 3.5 Å (e.g. 3.55 Å for a CO tip over pentacene in our calculation), atoms beyond the last two atoms on the apex are always over 5 Å away from the sample molecule if the last 3 atoms are aligned vertically. As a result, the contribution from these more distant atoms is small (e.g. Cu_3Cu above a CO tip contributes only 20%) and only gives a background signal with negligible corrugation. Hence, in the current geometry, the capability for high resolution can be attributed to the last two atoms on the apex. As shown above, CH_4 and pentacene tips yield similar images, giving an image typical of a C-H apex. A N_2 tip gives a resolution analogous to that of CO, because the N_2 molecule resembles CO and they have similar electronic structures at their ends. The second atom of Cl-terminated tips is farther away from the

sample than the C and N due to the larger Cl covalent radius. Cl_2 and CCl_4 have bond lengths around 2.0 Å and 1.8 Å, resp., yielding analogous resolution at similar height, and the Cl modified metal tip in the experiment successfully resolved the atomic structure of pentacene.[8] However, the difference between our simulated images obtained with CO and O_2 tips is large, and Cu_3CuO tip yields a completely different image. This is due to the small size of O, making the resolution more dependent on the second atom on the apex.

Beyond investigating the influence of modified tips on the resolution for a given sample molecule (pentacene), we may also ask whether the same level of spatial resolution can be expected for other sample molecules. Thus, we start with sample molecules that are similar to pentacene in having a network of planar C_6 rings, followed by molecules that have non-planar C_6 rings or chemical substitution. For consistency, we will use the CO tip defined above and the same imaging conditions to explore the achievable resolutions.

Coronene (Figure 5a) has a planar network of 7 fused C_6 rings, as shown in Figure 5a. The 7 C_6 rings are clearly resolved in the energy map, while the C-H bonds are less distinct than for pentacene (Figure 3c). The *IE* minima are located at the 7 hollow sites and local *IE* maxima are seen over the C_6 rings. It is interesting to find alternating *IE* minima and maxima on the edge of coronene, with a local minimum *IE* at the center of each C_3H_2 group (like the equivalent α site of pentacene) and a local maximum *IE* at the center of each C_2H_2 group (β site, like the equivalent sites at the two ends of pentacene). The local *IE* minima at the α sites and *IE* maxima at the β sites are also found at the long edges of the pentacene molecule image but not at the two β sites of its two extreme ends, which indicates how sensitive this imaging is to the local electronic structure.

While the planar C_6 networks of pentacene and coronene are imaged well, this is not true for benzene, with its single C_6 ring (Figure 5b). The energy image of the hexagonal C_6 ring of benzene takes the shape of an annulus of almost constant depth (oscillating by only about 10 meV, with the

slightly deeper values between the C atoms), surrounding a minimum at the central hollow site. The C-H bonds are invisible, immersed in a deep halo around the C_6 ring, while the outline of the molecular image is almost hexagonal. Benzene is the building block of planar C_6 networks. Hence, we find very similar *IE* hollows at the centers of C_6 rings in images of benzene, pentacene (Figure 3c) and coronene; however, the detailed shape of these C_6 ring images sensitively depends on the outer chemical structures, i.e., an outer C_3H_2 group helps to produce a hexagonal shape while a C_2H_2 group favors a circular shape.

We find that non-planar C networks also blur the AFM images of C_6 rings. Due to the rapid change of *IE* with distance (Figure 2a), the height window allowing the best resolution of atomic structure is quite small so that large spacings between layers of non-coplanar C atoms prevent obtaining a complete image. As an example, Figure 5c shows the energy image of C_{60} with a horizontal C_6 ring on its top exposed toward the tip: it presents a 3-fold rotation symmetry due to the alternation of outer C_5 rings and C_6 rings, which however are not themselves imaged; note also the strong difference in the C_{60} image compared to that for benzene. Figure 5d shows an energy map of a narrow (6, 0) carbon nanotube with strong curvature of each C_6 ring. The optimum height H = 2.95 Å here corresponds to the height between the O atom on the tip and the second plane of C atoms, comprised of C-C bond pairs parallel to the tube axis. Local *IE* maxima are found over the outermost C-C bonds, for which the smaller tip height of 2.62 Å results in intense maxima similar to the C-C bond images in Figure 3a; the *IE* minima are located at the C_6 hollows. It is seen that the rapidly changing *IE* values over the top C_6 rings produce a distorted image which does not directly suggest the atomic structure of carbon nanotube.

The electronic structure of defects also induces sensitive responses in the energy images. Here we consider substitution in planar C_6 rings. Such substitution may modify not only the electronic structure, but also the geometric structure, including a completely different bonding geometry to the substrate, which would be easily detected by AFM (and STM). So we limit ourselves here to the electronic effect, as may occur in relatively rigid or less-reactive molecules. In a pentacene molecule, we replace one C-H

group by a N atom (with the free molecular structure re-optimized), as shown in Figure 5e. The N substitution locally distorts the image, making it distinct from the image of the remaining C atoms. In our calculations with planar models, the same local image distortion was found, for the same tip height, following N substitution of C-H within other structures, e.g. within benzene (forming pyridine, Figure 5f) or within a graphene segment saturated by H atoms around the edge (such as coronene, substitution not illustrated). This result shows the potential of this technique for chemical identification within a single molecule. However, the high sensitivity has both advantages and disadvantages. The distortion yielded by the N defect blurs the image by reducing the contrast nearby. Additionally, this distortion may mix with the distortion due to other chemical structures and produce a complicated image. For example, it is almost impossible to identify the terpyridine molecule (Figure 5g, 2,6-bis(2-pyridyl)pyridine, consisting of 3 fused pyridines) from its energy map, where the three ends show the general character of pyridine while the chemical structure in between cannot be readily identified.

Conclusions

We have applied first principles calculations to explore the potential for high atomic resolution by AFM with various modified tips that terminate in a pair of atoms oriented perpendicularly to the sample molecule. We find that these last two apex atoms govern the contrast and only suitably selected tips can resolve the chemical structure of a pentacene molecule. Additionally, the electronic and geometrical structures of the sample molecules strongly affect the resolution. In our simulations, a CO tip can only well resolve the chemical structures of planar network of C_6 rings, but yields images which cannot be interpreted atomically for benzene, non-planar C rings, and C rings with defects. The high sensitivity of this approach depends on the electronic structures of the tip-sample pair, which could limit its applications due to requirement of careful selection for each sample of a suitable tip. On the other hand, when successful, this high resolution may be helpful to detect chemical behavior within a single molecule, due to a sensitive response to local electronic structure of the sample.

Acknowledgements

This work was supported in part by Hong Kong RGC Grant No. CityU 102408, and by the CityU Centre for Applied Computing and Interactive Media. CM is grateful to the French Consulate General in Hong Kong and Macau for financial support.

References

1. Eigler, D. M.; Schweizer, E. K., *Nature* **1990,** 344, 524-526.
2. Sugimoto, Y.; Abe, M.; Hirayama, S.; Oyabu, N.; Custance, O.; Morita, S., *Nat. Mater.* **2005,** 4, 156-159.
3. Binnig, G.; Quate, C. F.; Gerber, C., *Phys. Rev. Lett.* **1986,** 56, 930-933.
4. Ashino, M.; Schwarz, A.; Behnke, T.; Wiesendanger, R., *Phys. Rev. Lett.* **2004,** 93.
5. Ashino, M.; Obergfell, D.; Haluska, M.; Yang, S. H.; Khlobystov, A. N.; Roth, S.; Wiesendanger, R., *Nature Nanotech.* **2008,** 3, 337-341.
6. Sugimoto, Y.; Pou, P.; Abe, M.; Jelinek, P.; Perez, R.; Morita, S.; Custance, O., *Nature* **2007,** 446, 64-67.
7. Kaiser, U.; Schwarz, A.; Wiesendanger, R., *Nature* **2007,** 446, 522-525.
8. Gross, L.; Mohn, F.; Moll, N.; Liljeroth, P.; Meyer, G., *Science* **2009,** 325, 1110-1114.
9. Albrecht, T. R.; Grutter, P.; Horne, D.; Rugar, D., *J. Appl. Phys.* **1991,** 69, 668-673.
10. Ordejon, P.; Artacho, E.; Soler, J. M., *Phys. Rev. B* **1996,** 53, 10441-10444.
11. SanchezPortal, D.; Ordejon, P.; Artacho, E.; Soler, J. M., *Int. J. Quantum Chem.* **1997,** 65, 453-461.
12. Troullier, N.; Martins, J. L., *Phys. Rev. B* **1991,** 43, 1993-2006.
13. Kleinman, L.; Bylander, D. M., *Phys. Rev. Lett.* **1982,** 48, 1425-1428.
14. Perdew, J. P.; Burke, K.; Ernzerhof, M., *Phys. Rev. Lett.* **1996,** 77, 3865-3868.
15. Hamann, D. R., *Phys. Rev. B* **1989,** 40, 2980.
16. Feng, C.; Lin, C. S.; Fan, W.; Zhang, R. Q.; Van Hove, M. A., *J. Chem. Phys.* **2009,** 131.
17. We read the gray image with Matlab into a matrix which can be used to compare the gradation.
18. Giessibl, F. J.; Quate, C. F., *Phy. Today* **2006,** 59, 44-50.

Figure captions:

Figure 1. (Color on-line) (a) Model of the AFM tip with CO (gray and red atoms) at an Au apex atom of an Au_4 tetrahedron representing fcc Au (yellow atoms), the pentacene molecule (gray and white atoms for carbon and H, respectively), and 2 ML NaCl (purple and green atoms). (b) Energy line profiles along the long axis of the pentacene molecule with a tip consisting of Au_3Au alone (with substrate), combined Au_3Au-CO (with substrate or without substrate), and CO alone (without substrate). The energy line profile of Au_3Au-CO on the substrate (without pentacene) was also calculated at the same height. The atomic structure of the gas-phase pentacene molecule is shown to scale at bottom. The heights of the different parts of the tip are fixed.

Figure 2. (Color on-line) Height dependence of (a) the interaction energy *IE*, (b) the interaction force *IF* and (c) the frequency shift *FS* of a CO tip over different sites (marked in d) of a pentacene molecule. (d) Ball-and-stick model of the pentacene molecule, with some sites labeled following IUPAC numbering and others denoted with colored points. (e) Experimental AFM image [from Gross, L.; Mohn, F.; Moll, N.; Liljeroth, P.; Meyer, G., *Science* **2009,** 325, 1110-1114; reprinted with permission from AAAS] and (f) calculated *IE* map at a CO height of 2.7 Å above the pentacene. The gray scale of the *IF* and *IE* maps is shown at bottom.

Figure 3. (Color on-line) Interaction energy *IE* maps of a pentacene molecule with CO tip heights above the pentacene of (a) 2.4 Å, (b) 2.7 Å, (c) 2.95 Å, and (d) 3.4 Å. Color contrast is used to emphasize the interesting resolution information. While red and blue denote low and high *IE* values, resp., the color ranges are independently adjusted in each panel.

Figure 4. (Color on-line) *IE* line profiles along the long axis and *IE* maps of the pentacene molecule yielded by tips terminated in (a) CH_4, (b) CCl_4, (c) O_2, (d) Cu_3CuO, (e) N_2, and (f) Cl_2. The tip heights of the line profiles are shown in the insets (in Å). The line profiles are calculated at four different heights around the height giving the minimum *IE* at the central hollow site. The *IE* maps

are produced at a "best-resolution height" which is the average value of the heights at which *IE* minima occur at different positions shown in Figure 2d.

Figure 5. (Color on-line) The atomic structure and *IE* map yielded by a CO tip for H=2.95 Å of (a) coronene, (b) benzene, (c) fullerene, (d) (6, 0) carbon nanotube, (e) pentacene with one C substituted by a N atom, (f) pyridine, and (g) terpyridine. The scales of each structure and image pair are the same.

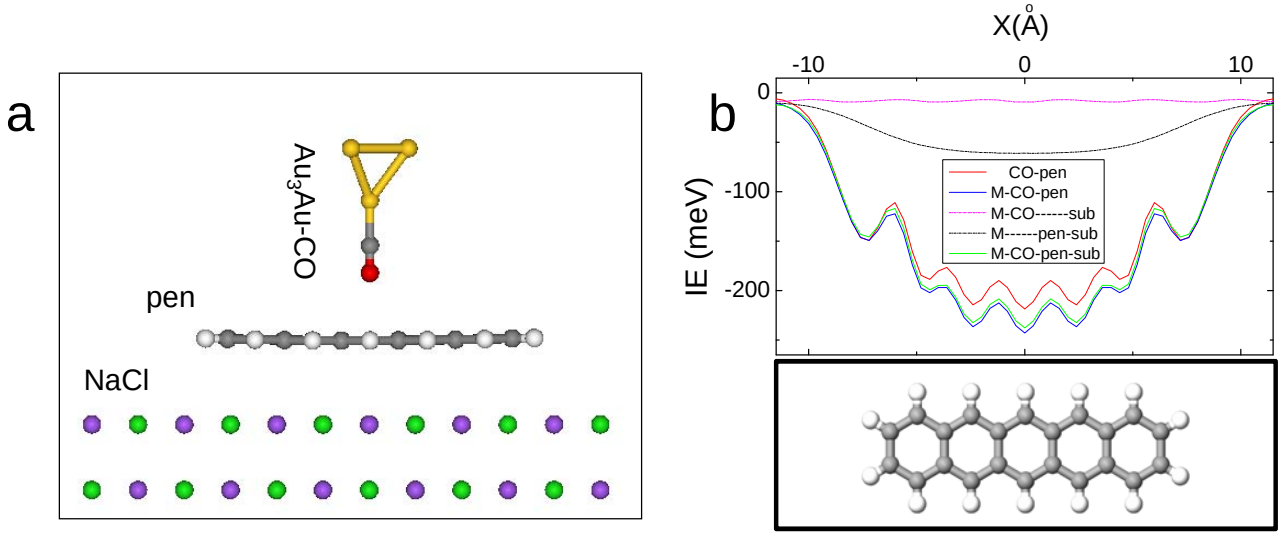

Figure 1. C.S. Guo, M.A. Van Hove, et al.

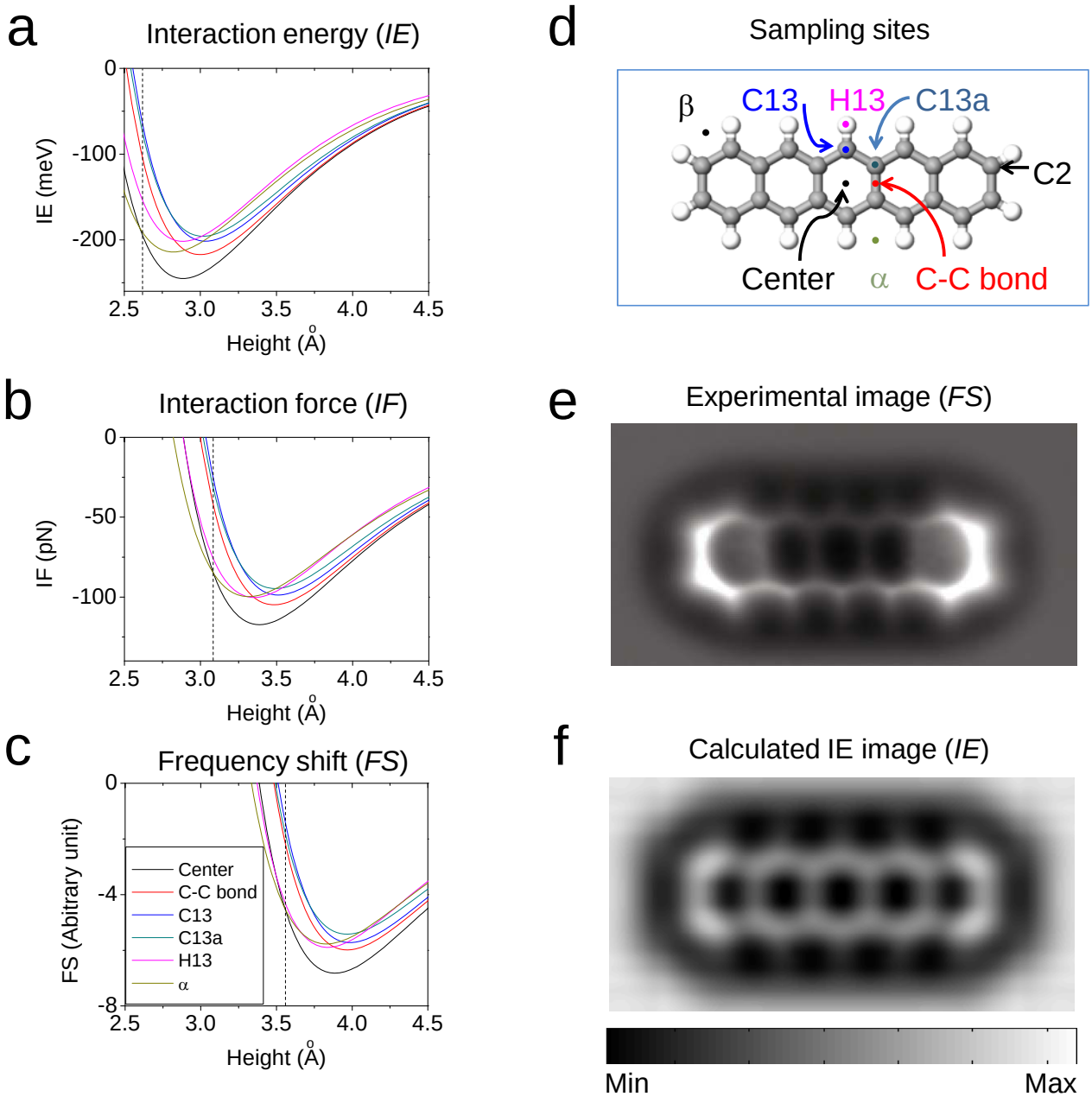

Figure 2. C.S. Guo, M.A. Van Hove, et al.

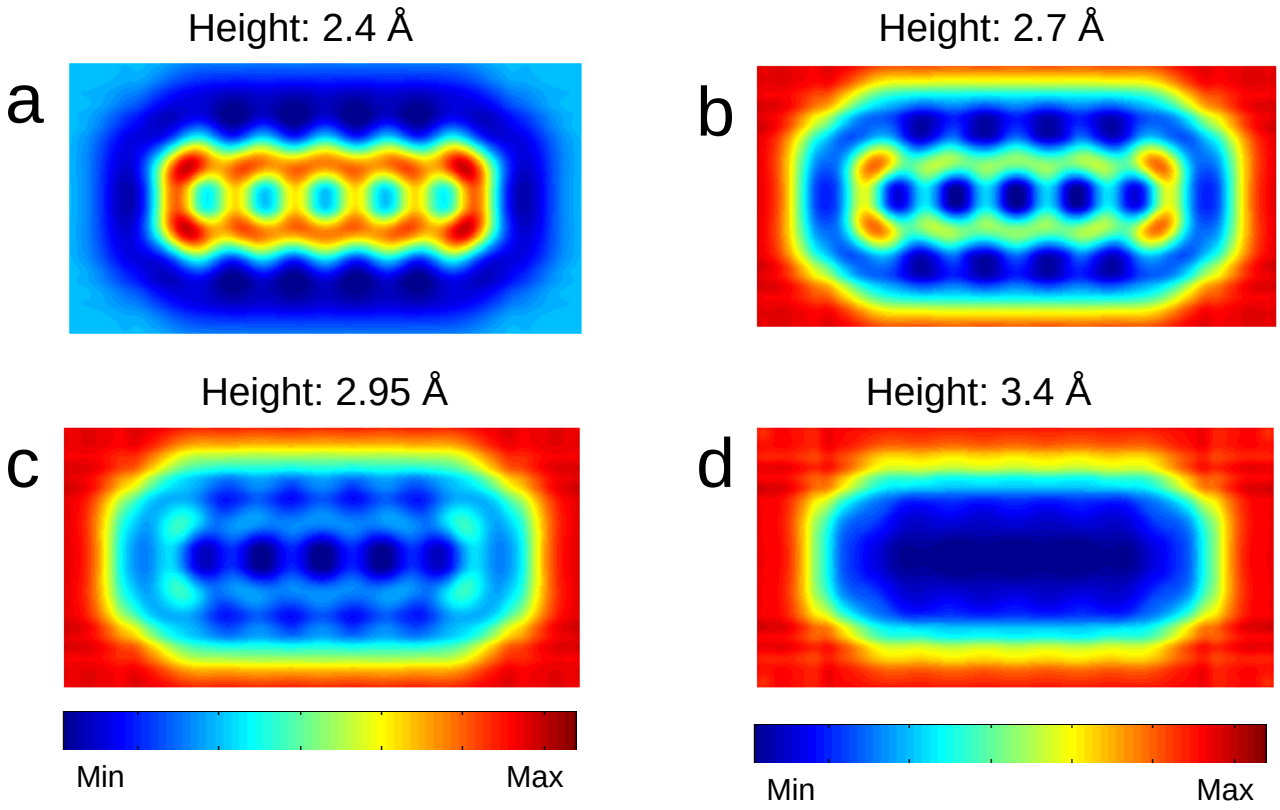

Figure 3. C.S. Guo, M.A. Van Hove, et al.

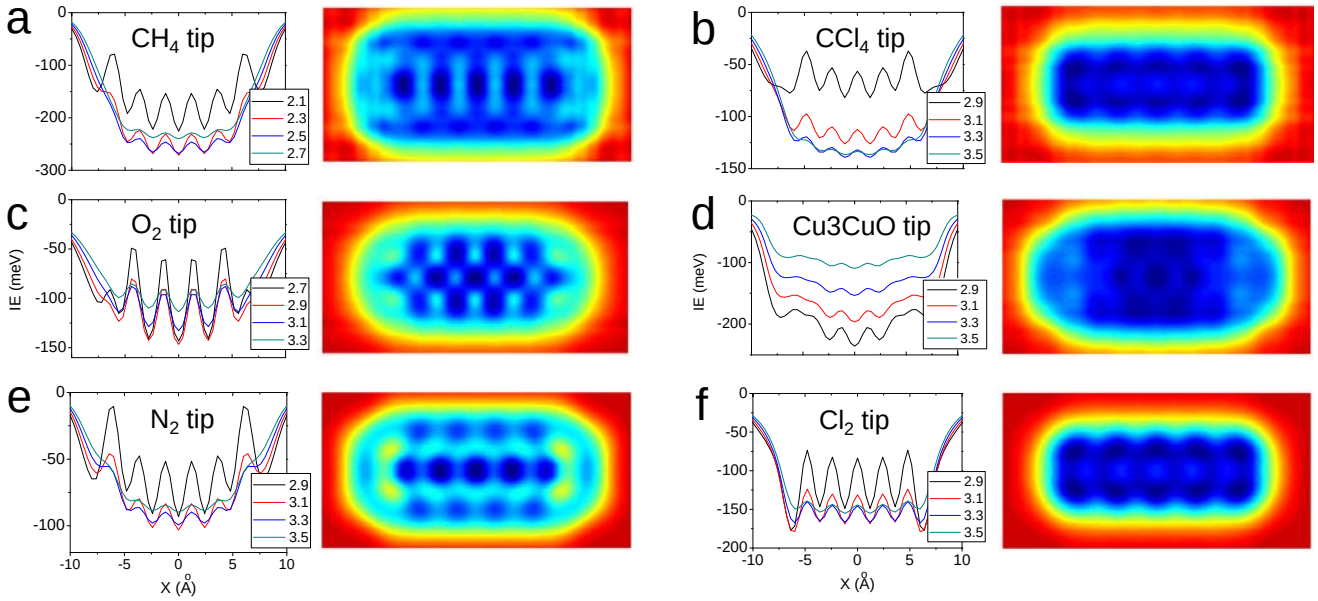

Figure 4. C.S. Guo, M.A. Van Hove, et al.

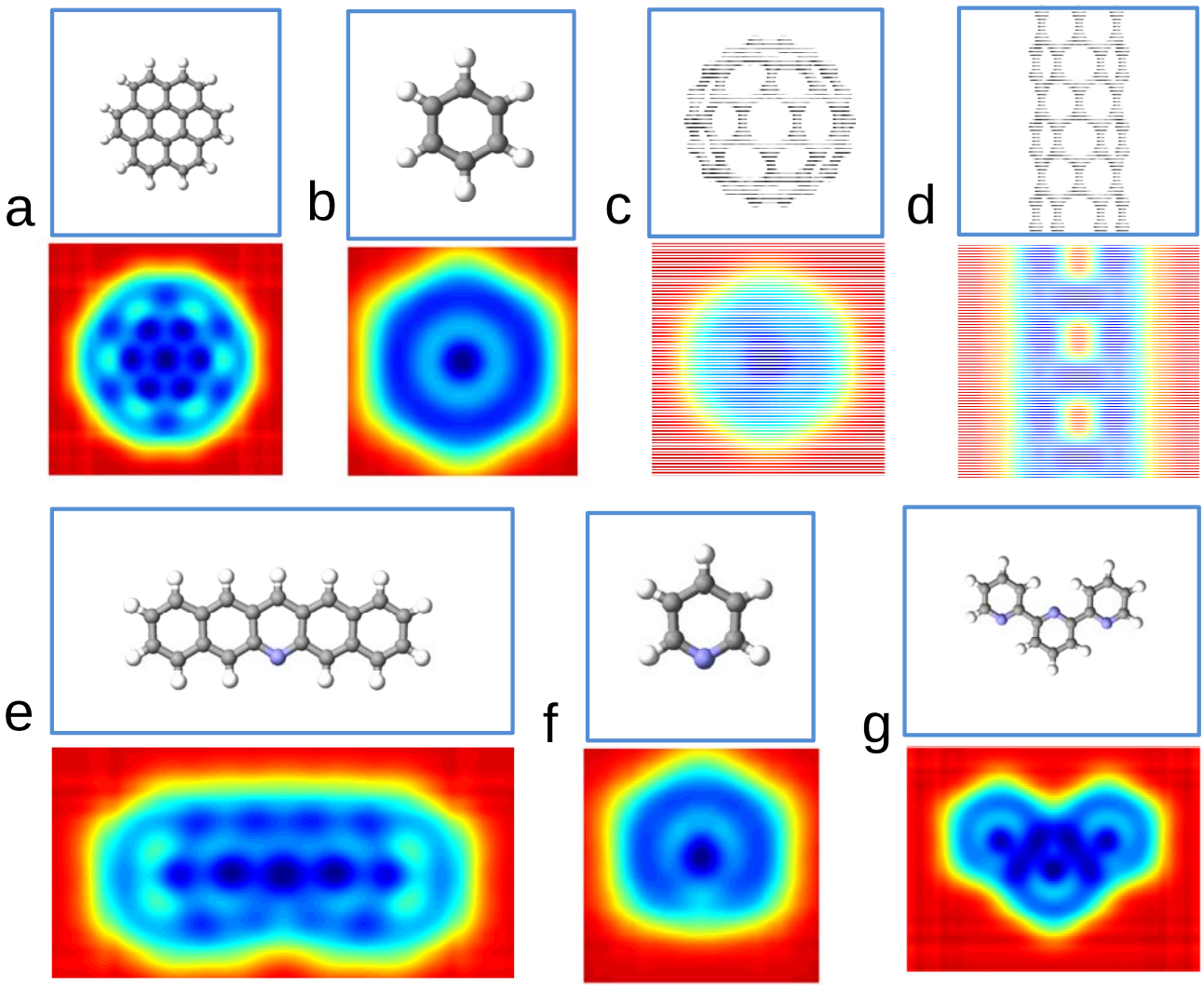

Figure 5. C.S. Guo, M.A. Van Hove, et al.